ARMA 17-515

Bio-inspired fluid extraction model for reservoir rocks

Fernando Patino-Ramirez
Georgia institute of technology, Atlanta, GA, USA.
Chloe Arson
Georgia institute of technology, Atlanta, GA, USA.

ABSTRACT: Biological and engineering flow systems maximize their efficiency by following the path of minimum energy over the domain they are embedded in. This fact motivates the present research, since industrial fluid extraction and injection processes are designed to minimize the implementation cost (energy, materials) and maximize the volume of fluid injected (or withdrawn). This work presents a bio-inspired fluid flow model to optimize the path that connects resource-rich pores in a rock. We explain the commonalities between the equations governing flow in a porous medium and growth of slime mold, an organism that dynamically deploys tube-like structures and adapts them as a function of their contribution to the overall network. We perform several simulations to analyze the influence of the pore size distribution and of pore spatial distribution on the topology of the extraction network predicted by the slime mold growth algorithm. We discuss the suitability of the biomimicry model to design fracture patterns for optimal fluid extraction from a porous rock.

1. INTRODUCTION

What fracture network topology optimizes fluid flow in a rock mass? Power laws and fractal dimensions govern most physical processes observed in nature. However, optimization algorithms that shape natural self-organization remain in many cases unknown. Furthermore, engineering approaches rarely consider nature as a guide to improve human systems and very few attempts have been made to explain the fractal nature of the topology observed in many connectivity networks.

The constructal theory (Bejan & Errera, 1997) is an optimization method for finite flow systems with configuration (e.g., slenderness), in which a purpose (e.g., heat collection) and constraints to the flow (e.g. mass balance) are established. This theory can be used to predict the topology of both natural networks, such as the design of the lungs (a H Reis, Miguel, & Aydin, 2004), and man-made networks, such as the layout of cities (Bejan & Lorente, 2008; a. Heitor Reis, 2006). Unlike other biological models of cell networks, the constructal theory is completely deterministic, predicting the layout of a network without prior assumptions. Major limitations are: (a) the need to assume controlling thermodynamic potentials, steady boundary conditions and uniform distribution of connecting points; (b) the absence of interaction dynamics from the formulation which disregards the fluctuations of the environment and the corresponding adaptation of the network. In the same way, Steiner tree algorithms allow finding: The minimum spanning tree from a set of points distributed in space; The global optimum from the creation of Steiner points that minimize the length needed to connect 3 points on the plane; The minimum network length concatenating those full Steiner trees using a combinatorial algorithm (Winter & Zachariasen, 1997).

The astonishing similarities noted between the geometry of networks formed by living organisms (e.g. roots and bacteria) and that of infrastructure facilities (e.g. railway systems, see (Adamatzky, De Baets, & Van Dessel, 2012; Tero et al., 2010) inspired the present study. We follow the growth principles of true slime mold (Physarum polycephalum), an intelligent organism that yields better solutions than Steiner trees for network configuration (Toshiyuki Nakagaki, Yamada, & Hara, 2004) and is capable of changing its topology over time, depending on the variability in topological and environmental conditions. Using a slime mold growth algorithm, we calculate the size of each crack that connects pores in a rock mass in order to maximize the extraction of a fluid from those pores. We first explain the principle of the bio-mimicry model used for fluid flow. We then study homogeneous and heterogeneous rock microstructures, with different pore size

distributions. Lastly, we recommend designs of fracture patterns for optimal extraction from porous rocks.

2. BIOLOGICAL ANALOG OF FLUID FLOW

2.1. Governing equations of the bio mimicry model

We construct a biomimicry flow network model, in which the porous medium is represented by a distribution of pores (nodes) of various sizes. Cracks (edges) connect the pores and allow the flow of fluid from the pores (sources) to a sink point. The width of the cracks connecting pores is calculated based on a mathematical model that mimics the growth behavior of *Physarum plucephalum*. This amoeba-like organism is a single cell consisting on a dendritic network of tubular elements that ensure the flow of nutrients and signals through the plasmodium (T Nakagaki, Yamada, & Tóth, 2000). The organism spreads uniformly under constant environmental conditions and adapts dynamically due to the composition of the substrate, the supply of light, the distribution of food spots and the presence of physical barriers that restrict growth (Tero et al., 2010).

Physical observation shows that the placement of a food source on certain locations of the network induces tube shrinkage and thickening, since flux through a tube strengthens it, while unused tubes tend to degenerate and disappear. The mathematical formulation of the present model follows the empirical rules established by (Tero, Kobayashi, & Nakagaki, 2007), where tubes that are not part of the flow network tend to disappear, and, when two or more paths connect the same set of food spots, only the shortest prevails.

Flow through tubes is assumed to follow the Hagen-Poiseulle equation, which states that the flux along a given tube Q_{ij} can be expressed as:

$$Q_{ij} = \frac{\pi r_{ij}^4}{8\eta} \cdot \frac{p_i - p_j}{L_{ij}} \tag{1}$$

Where η is the dynamic viscosity of the fluid (assumed to be water in the present study, for simplicity), p_i and p_j are the pressures at nodes i and j respectively, r_{ij} and L_{ij} are the radius and the length of the tube, respectively. The conductivity of the tube is defined as:

$$D_{ij} = \frac{\pi r_{ij}^4}{8\eta} \tag{2}$$

The conductivity of the tube (edge representing a crack) changes when the radius of the tube changes. The length remains constant, and the pressure at each node is computed from the principle of mass conservation:

$$\sum_i^n Q_{ij} = 0 \tag{3}$$

The flux is set as $-I_{ij}$ and I_{ij} for nodes set as sink and source, respectively. The value of I_{ij} is proportional to the volume of the pore (node).

The resulting linear system of equations is solved for p_i and Q_{ij}. The change of tube conductivity within a time step n is given by the following expression (Tero et al., 2007):

$$\partial D_{ij} \Big/ \partial n = \frac{\left(q_{ij} \Big/ q_m \right)^\gamma}{1 + \left(q_{ij} \Big/ q_m \right)^\gamma} \mu_{Dij} - r D_{ij} \tag{4}$$

Where q_{ij} is the flux through the tube during step n, q_m is the mean flux trough the network, μ_{Dij} is the mean conductivity of the network. γ is the parameter that describes the nonlinearity of the growth feedback and is set as 1.8 according to (Tero et al., 2010) and r is the decay rate of the tube (set as 2%).

2.2. Slime mold growth algorithm

The model consists of a two dimensional, regular, triangular lattice mesh: the coordination number of a node is equal to 6, i.e. each node is connected to 6 other nodes by 6 throats that are 60° apart from each other. The grid contains n_x x n_y nodes, where n_x and n_y are the numbers of nodes along the x and y-axis, respectively. Each node represents a spherical pore inside the rock mass. Each edge that connects two pores represents a pore throat, modeled as a slime mold tube, which is assumed to be a cylinder. We assume that pore and pore throats follow independent normal size distributions. The parameters of the initial probability density functions are taken from published articles about reservoir rocks. Node (pore) radius distributions do not vary during the simulations, but the radii of the cylindrical edges are optimized by using the slime mold growth algorithm.

After generating the mesh and assigning the initial size distributions to the nodes and edges, n nodes (pores) are selected to play the role of flow sources. The probability of choosing a pore is proportional to its size, for instance the probability of selecting a pore of radius $2r$ is twice the probability of choosing a pore of radius r. At each computational step, we chose n equal to $0.5 n_x n_y$ sources, which yielded a realistic network topology within a simulation time shorter than a day. Larger sets

of sources did not yield significant changes in the topology of the system.

At each step of the computation, different sets of sources are considered but the sink point remains at the same location, at the top center of the domain ($i = 1$ and $j = 0.5n_x$). Next, the corresponding flux input and output are set according to the volume of the source pore, and the node pressures and edge flux values are obtained from the corresponding set of linear equations. Then, the conductivity and radius of each edge is updated and a set of nodal sources is considered.

3. BIO INSPIRED OPTIMIZATION OF FLUID EXTRACTION FROM POROUS ROCKS

3.1. Mesh and boundary conditions

The simulations presented in the following were all done with the same lattice mesh, with $n_x = 50$ and $n_y = 70$. The scaling factor of the mesh (which defines the length of each edge) was set as 1, i.e. the mesh is considered non-dimensional according to the growth mechanism defined by (Tero et al., 2007).

The microstructure parameters where chosen according to (Gao, Li, & Yang, 2016) for a sample of Lithic feldspar sandstone in a tight oil reservoir. The pore radius is distributed normally with a mean value $\mu_p = 145\mu m$ and a standard deviation $\sigma_p = 35\mu m$; the pore throat mean radius is $\mu_t = 0.48\mu m$ with a standard deviation of $\sigma_p = 0.12\mu m$.

3.2. Microstructure models

We design different microstructure models to evaluate the influence of the variability of the pore and pore throat size distributions on the deployment of the slime mold inspired flow network. We study: The influence of the mean value and standard deviation of the pore (node) size distribution; The influence of the spatial variability of the pore sizes.

3.2.1. Influence of pore mean size on network topology

The three microstructures described in Table 1 were compared to study the effect of the variation of the mean pore size distribution on the development of the flow network.

Table 1. Effect of pore mean size

Model	Mean (μ) [ηm]	Std. Dev (σ) [ηm]
1	μo=145	35
2	2μo=290	35
3	3μo=435	35

3.2.2. Influence of pore size variability on network topology

In order to assess the influence of the standard deviation of the pore size distribution, four microstructures, described in Table 2, were compared. The mean pore size was kept constant as well as the pore throat size distribution parameters.

Table 2. Effect of pore size standard deviation

Scenario	Mean (μ) [ηm]	COV [%]	Std. Dev (σ) [ηm]
1	145	5	7.25
2 (Base)	145	24.14	35.00
3	145	50	72.50
4	145	100	145

3.2.3. Influence of pore size spatial distribution on network topology

In order to understand the influence of the spatial distribution of pores on the deployment of the network, three different cases were considered, as explained in Table 4 and Figure 1. In each case, the domain is made of a combination of regions of different mean pore size, but same standard deviation. In case A, the whole domain has a low mean pore size. In case B, the lower half of the domain has a mean pore size three times higher than the upper half. In case C, the mean pore size is higher in the upper half than the lower half. The position of the sink is the same in all three cases: at the top center of the domain.

Table 3. Effect of pore space distribution

Pore Size Distribution	Mean (μ) [ηm]	Std. Dev (σ) [ηm]
PSD-1	μo=145	35
PSD-2	3μo=435	35

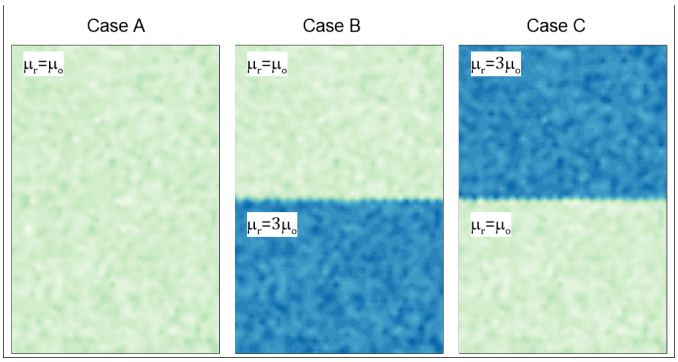

Figure 1. Cases studied for spatial pore size distribution

4. RESULTS

We compare the topology of the initial porous network (with pores and pore throats of given initial size distributions placed on the grid) to that of the final network, obtained after using the slime mold growth algorithm. Within the final network, we define a

preferred flow path, as follows. The 10% larger edges obtained at the end of the simulation are selected (note that larger edges are tubes that are were selected the highest number of times to ensure flow from a set of pore source to the sink). Within the set of 10% larger edges, clusters of connected tubes are identified. In all simulations, one cluster contained 90% of the larger edges. This cluster defines the preferred flow path.

4.1. Influence of pore mean size on network topology

The average growth of tube (edge) radius was computed for edges within the entire domain and within the preferred path only. Results are summarized in Table 4. The growth rate of the edges within the preferred path is about five times higher than the average growth rate within the entire domain.

Table 4. Mean increase of edge radii with varying mean pore size

Mean increase of pore radii	Every edge	Preferred path edges
μo	3.42%	16.39%
2μo	3.52%	16.92%
3μo	3.39%	16.30%

The results show no significant differences between the increase of edges radii; this fact can be explained by the nature of the algorithm, which is sensitive only to the relative weight (size) the source points (pores) over the domain. Since the probability density function and standard deviations are the same in the three microstructure models tested, the variability of mean pore size does not affect the topology of the flow network generated with the slime mold growth algorithm. We check that the ratio "total volume of the pores connected by the edges forming the preferred path / total volume of pores in the domain" is the same in the three simulations (Table 5). This result confirms that the same volume fraction of resources can be extracted through the preferred flow path in all cases.

Table 5. Effect of mean pore size on preferred path efficiency

Mean pore Size	μo	2μo	3μo
% Of total pore volume connected by the preferred path	27.07%	26.59%	27.13%

4.2. Influence of pore size variability on network topology

Table 6 summarizes the edge growth rates within the entire domain and within the preferred path, for microstructures with different pore size standard deviations (described in Table 2). Table 7 shows the porous volume accessible by the preferred path. We note only slight differences in the four simulation results. This is because pore sizes are centered around the mean pore size. The probability of selecting a pore in a set is not strongly affected by the variability of the pore size distribution. Therefore the edges connecting the pores are used with similar probability regardless of pore size standard deviation, which leads to similar network topologies.

Table 6. Mean increase of edge radii as a function of pore size standard deviation

COV of pore size distribution	Every edge	Preferred path edges
5%	3.38%	15.90%
24.14%	3.50%	17.08%
50%	3.30%	15.60%
100%	3.94%	18.64%

Table 7. Effect of pore size standard deviation on preferred path efficiency

COV	5%	24.14%	50%	100%
% Of total pore volume connected by the preferred path	26.75%	26.22%	24.98%	26.07%

4.3. Influence of pore size spatial distribution on network topology

The final networks obtained for the three microstructures described in Table 3 and Figure 1 (Cases A, B and C) are shown in Appendix 1. The creation of preferential paths for fluid extraction is analyzed in terms of relative growth or shrinkage of the edges (percentage of variation of radius size). Results are plotted as heat maps where each edge is represented as a point located on its middle point.

Tables 8-10 summarize the analysis of network connectivity, i.e. the average radius growth within the entire domain and within the preferred path only.

Table 8. Mean increase of edge radii – Case A

Mean increase of edge radii	Every edge	Preferred path edges
Entire Domain	3.14%	14.73%
Upper Half	3.54%	15.86%
Lower Half	2.73%	13.22%

Table 9. Mean increase of edge radii – Case B

Mean increase of edge radii	Every edge	Preferred path edges
Entire Domain	6.78%	33.32%
Upper Half	6.79%	36.68%
Lower Half	6.76%	30.08%

Table 10. Mean increase of edge radii – Case C

Mean increase of edge radii	Every edge	Preferred path edges
Entire Domain	1.51%	6.93%
Upper Half	1.79%	7.23%
Lower Half	1.23%	6.20%

From the obtained results it is possible to see that, as expected, the increase of the edge radii is significantly higher on the preferred path compared to the complete set of edges (around 5 times higher). Within both the entire domain and the preferred path, the highest increase is seen in Case B, where the higher concentration of pore (and resource) volume is far away from the sink. Tube growth is needed to increase conductivity and reach the resources in the lower part of the domain.

Case C presents the smaller increase of edge radii overall, which can be attributed to the spatial distribution, where the biggest concentration of the resources is already close to the sink. There is no significant incentive to enhance flow far away from the sink according the slime mold growth algorithm.

Finally, we note an important difference of growth rate between zones: the growth rate is always greater on the upper half compared to the lower one; this result can be explained by the necessary to deploy a network of low resistance to the flow at the vicinity of the sink.

Tables 11-13 summarize the analysis of preferred path efficiency within the entire domain and within each zone.

Table 11. Volume fraction of pores connected by the preferred path - Case A

Location	% From total domain pore volume	% Of total pore volume connected by the preferred path	Efficiency
Full domain	100%	27.01%	27.01%
Upper half	50.01%	15.59%	31.17%
Lower half	49.99%	11.42%	22.86%

Table 12. Volume fraction of pores connected by the preferred path - Case B

Location	% From total domain pore volume	% Of total pore volume connected by the preferred path	Efficiency
Full domain	100%	26.83%	26.83%
Upper half	11.12%	3.00%	26.98%
Lower	88.88%	23.83%	26.81%

Location	% From total domain pore volume	% Of total pore volume connected by the preferred path	Efficiency
half			

Table 13. Volume fraction of pores connected by the preferred path - Case C

Location	% From total domain pore volume	% Of total pore volume connected by the preferred path	Efficiency
Full domain	100%	32.84%	34.84%
Upper half	88.90%	31.16%	35.05%
Lower half	11.11%	1.68%	15.12%

In Tables 11-13, the first column shows the distribution of the pore volume in the domain. By definition, the sum of the pore volume fractions in the upper and lower halves equals the pore volume fraction in the entire domain, i.e. 100%. In the same way, the sum of the volume fraction of pores connected by the preferred path in the upper and lower halves equals the volume fraction of pores connected by the preferred path over the entire domain. The efficiency is defined as the ratio between the pore volume connected by the preferred path and the total pore volume available in a given area.

Results show that with less than 10% of the edges of the domain, the computed network is able to reach around 30% of the total pore volume available, with similar results even for strongly heterogeneous distributions of total pore volume. Furthermore, the results show that the highest value of efficiency is obtained for Case C, where the resources are closer to the sink, similarly to the results obtained for mean increase of edge radii.

On the other hand, the lowest efficiency (26.83%) is obtained in Case B, where the majority of the resources are away from the sink, which also agrees with the results obtained for edge radii increase. Once again it was observed that the efficiency is always higher on the upper half of the domain, where at the same time the preferred path shows highest radii increase as well. These results show the importance of network topology for efficient extraction of resources from porous rocks, through main veins connected directly to the sink.

5. CONCLUSIONS

We construct a biomimicry flow network model, in which the porous medium is represented by a distribution of pores (nodes) of various sizes. Pores represent source points, and a sink point is placed at the top center point of the domain. The size of the cracks (edges) connecting pores is calculated based on a mathematical model that mimics the growth behavior of

Physarum plucephalum. The algorithm selects flow paths that preferably connect the larger pores. Edges along these flow path grow in size as a function of the number of times they are selected for conveying fluid flow from the pores to the sink. We compare the topologies of networks generated with different pore size distributions. In all cases, a unique preferred flow path can be identified. The top 10% larger edges connect pores that represent 25% to 32% of the total pore volume. The growth rate of edges within the preferred path is five times higher than the average growth rate of the edges in the entire domain of study. Edges tend to grow in size when they are closer to the sink.

The slime mold inspired porous networks maximize fluid extraction. The results obtained show the potential to model real distributions of resources within porous media, in order to find the optimal flow path based on slime mold growth; for this reason, further research on this topic will include benchmarking between fracture patterns observed in the field versus the bio-inspired network, in order to validate the effectiveness of the method.

Finally, it is important to mention that specific calibration for this application is needed, since the growth law adopted in the present article is directly taken from a biological model. Even though this choice is qualitatively suitable for the analysis, further research will include the development of physical experiments on slime mold.

ACKNOWLEDGEMENTS

This research was funded by the Engineering Research Center on Bio-Inspired and Bio-mediated Geotechnics (CBBG), supported by the U.S. National Science Foundation (grant # 1449501).

REFERENCES

Adamatzky, A., De Baets, B., & Van Dessel, W. (2012). Slime mould imitation of Belgian transport networks: Redundancy, bio-essential motorways, and dissolution. *International Journal of Unconventional Computing*, *8*(3), 235–261.

Bejan, A., & Errera, M. R. (1997). Deterministic Tree Networks for Fluid Flow: Geometry for Minimal Flow Resistance Between a Volume and One Point. *Fractals*, *5*(4), 685–695. https://doi.org/10.1142/S0218348X97000553

Bejan, A., & Lorente, S. (2008). Design with Constructal Theory. *Design with Constructal Theory*, (September), 1–529. https://doi.org/10.1002/9780470432709

Gao, H., Li, T., & Yang, L. (2016). Quantitative determination of pore and throat parameters in tight oil reservoir using constant rate mercury intrusion technique. *Journal of Petroleum Exploration and Production Technology*, *6*(2), 309–318. https://doi.org/10.1007/s13202-015-0186-6

Nakagaki, T., Yamada, H., & Hara, M. (2004). Smart network solutions in an amoeboid organism. *Biophysical Chemistry*, *107*(1), 1–5. https://doi.org/10.1016/S0301-4622(03)00189-3

Nakagaki, T., Yamada, H., & Tóth, A. (2000). Maze-solving by an amoeboid organism. *Nature*, *407*(6803), 470. https://doi.org/10.1038/35035159

Reis, a. H. (2006). Constructal Theory: From Engineering to Physics, and How Flow Systems Develop Shape and Structure. *Applied Mechanics Reviews*, *59*(5), 269. https://doi.org/10.1115/1.2204075

Reis, a H., Miguel, a F., & Aydin, M. (2004). Constructal theory of flow architecture of the lungs. *Medical Physics*, *31*(5), 1135–1140. https://doi.org/10.1118/1.1705443

Tero, A., Kobayashi, R., & Nakagaki, T. (2007). A mathematical model for adaptive transport network in path finding by true slime mold. *Journal of Theoretical Biology*, *244*(4), 553–564. https://doi.org/10.1016/j.jtbi.2006.07.015

Tero, A., Takagi, S., Ito, K., Bebber, D. P., Fricker, M. D., Yumiki, K., … Nakagaki, T. (2010). Rules for Biologically Inspired Adaptive Network Design. *Science*, *327*(January), 439–442. https://doi.org/citeulike-article-id:6578033

Winter, P., & Zachariasen, M. (1997). Euclidean Steiner minimum trees: An improved exact algorithm. *Networks*, *30*(3), 149–166. https://doi.org/10.1002/(SICI)1097-0037(199710)30:3<149::AID-NET1>3.0.CO;2-L

APPENDIX 1

The following set of figures shows the topologies found on the section 4.3 regarding the edges network. The intensity of the color is related to the relative growth of the given edge within the domain.